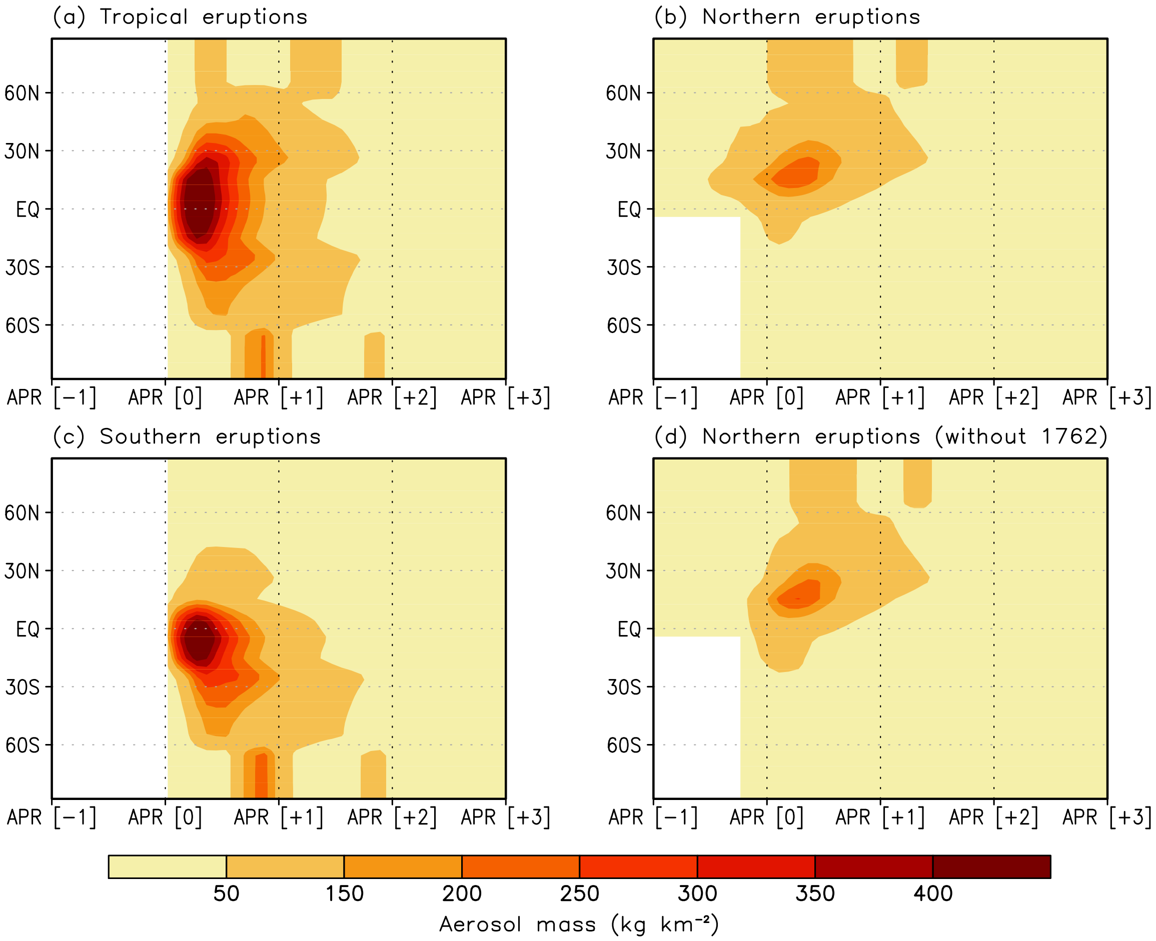

Figure S1: Temporal composites of column integrated volcanic aerosol mass following (a) tropical, (b) northern and (c) southern eruptions. (d) Same as (b) but from five northern eruptions without 1762 Laki eruption. Shadings presented only where volcanic aerosols exist.

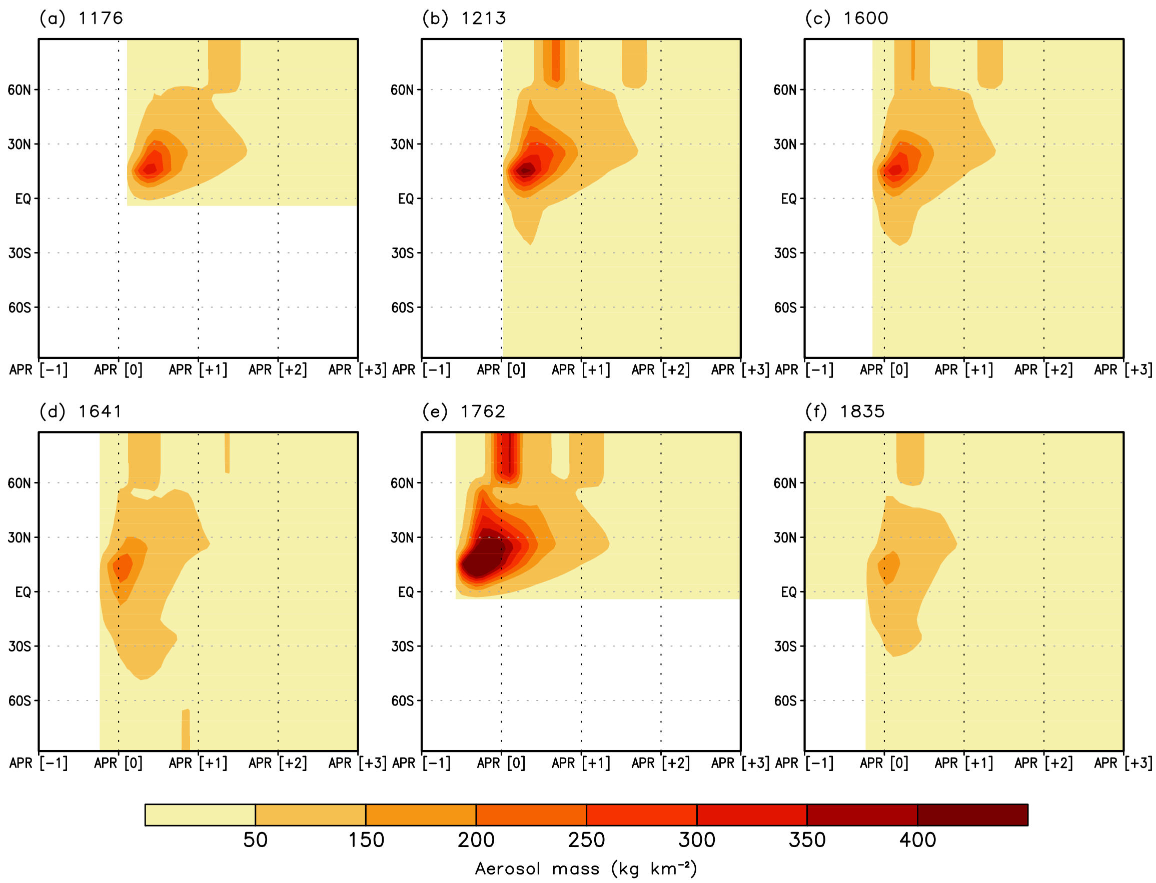

Figure S2: Same with Fig. S1, but from individual northern eruptions. Shadings presented only where volcanic aerosols exist.

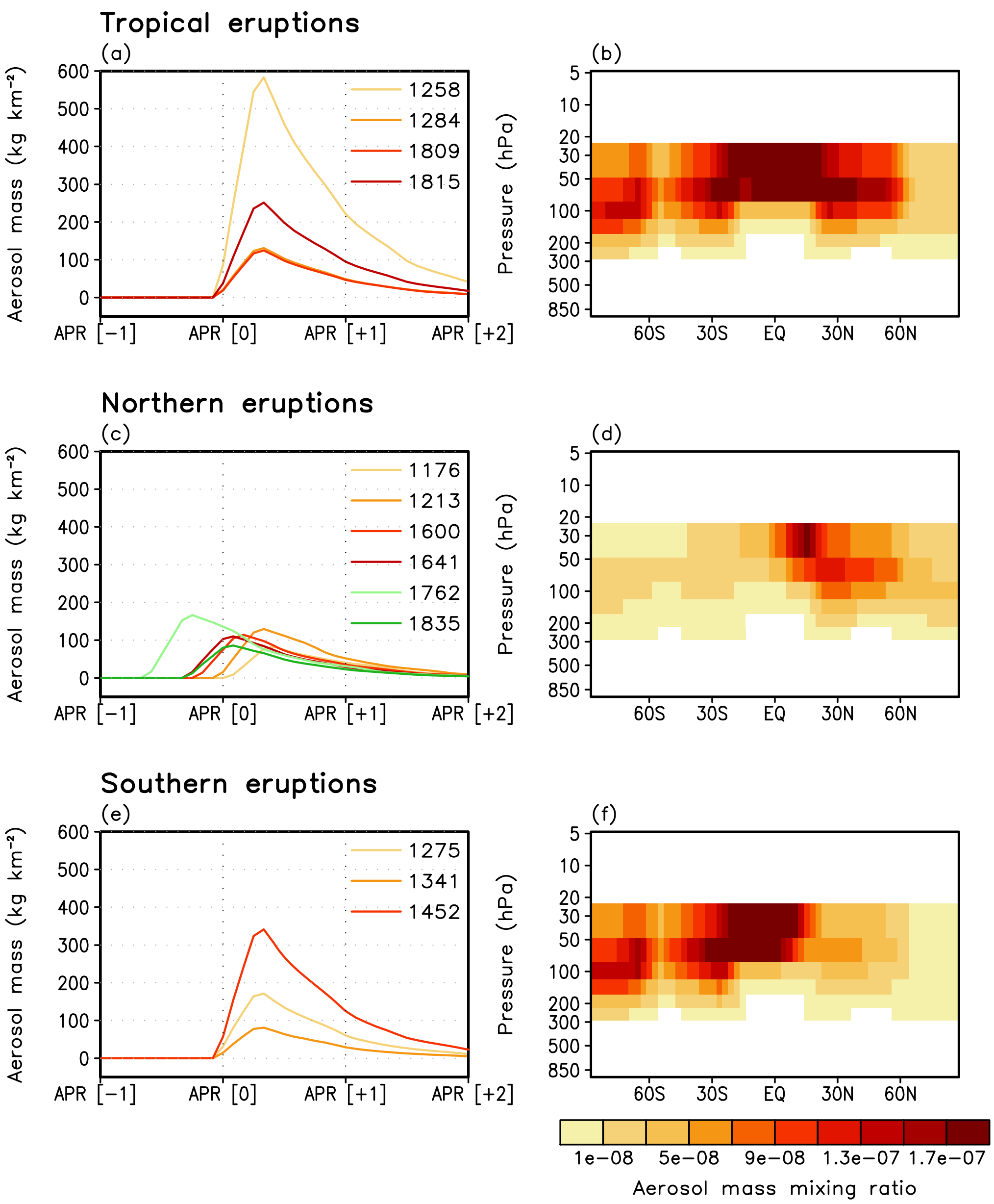

Figure S3: (a,c,e) Global averaged volcanic aerosol mass injection amount from individual (a) tropical, (c) northern and (e) southern eruptions. (b,d,f) Composites of vertical distribution of volcanic aerosol mass injection from (b) tropical, (d) northern and (f) southern eruptions during boreal winter of YR0 (December of YR0 to February of YR+1). Shadings presented only where volcanic aerosols exist.

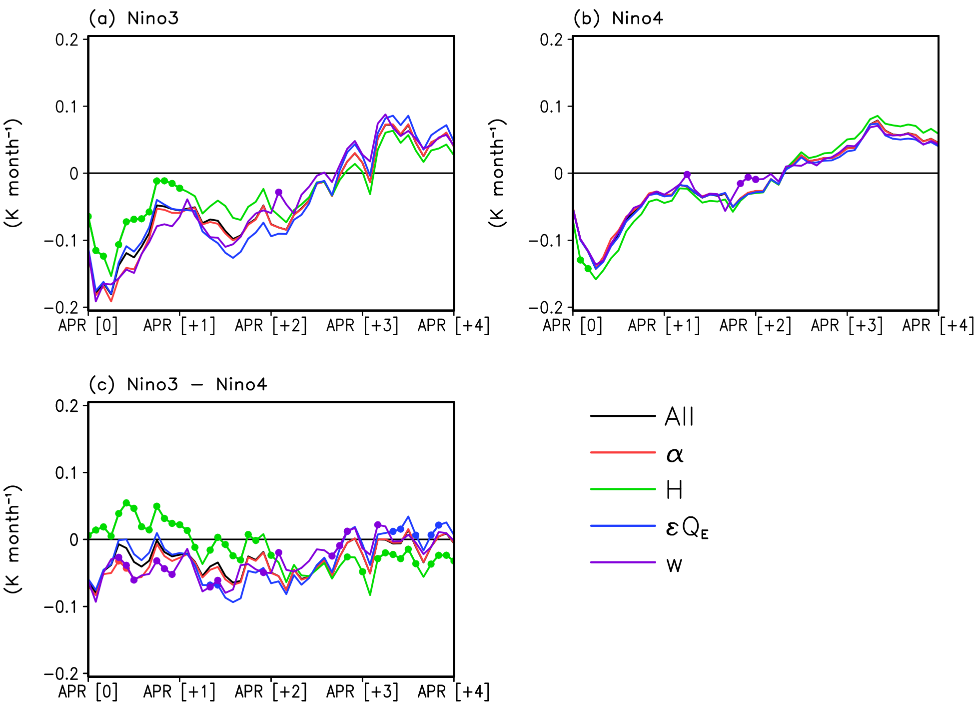

Figure S4: Mixed layer temperature budget analysis from

$$\frac{dT'(x,y)}{dt} = \frac{Q'[1 - \bar{\alpha}(x,y)]}{c_p \rho_o H(x,y)} - \frac{\varepsilon \bar{Q}_E(x,y) T'(x,y)}{c_p \rho_o H(x,y)} - \bar{w}(x,y) \frac{\partial T'(x,y)}{\partial z}$$

following McGregor and Timmermann (2011), over (a) Niño3 (150–90°W, 5°S to 5°N), (b) Niño4 (160°E to 150°W, 5°S to 5°N) regions and (c) the difference between the two regions. c_p and ρ_o are specific heat of seawater at constant pressure and the density of water, respectively. Q' is volcanic eruptions induced solar radiation anomalies. Results from spatially varying climatology (pre-eruption five-years mean) of $\bar{\alpha}$ (albedo), H (mixed layer depth; provided from CESM-LME with defining following Large et al., 1997), $\varepsilon \bar{Q}_E$ (Newtonian cooling) and $\bar{w}$ (mean upwelling) (All, black) and from spatially uniform (average of Niño3 and Niño4 regions) $\bar{\alpha}$ (red), H (green), $\varepsilon \bar{Q}_E$ (blue), and $\bar{w}$ (purple) are displayed. Dots indicate statistically significant differences at the 5% level from All.

Large, W. G., Danabasoglu, G., Doney, S. C., and McWilliams, J. C.: Sensitivity of surface forcing and boundary layer mixing in a global ocean model: Annual-mean climatology, J. Phys. Oceanogr., 27, 2418–2447, https://doi.org/10.1175/1520-0485(1997)027<2418:STSFAB>2.0.CO;2, 1997.

McGregor, S. and Timmermann, A.: The effect of explosive tropical volcanism on ENSO, J. Climate, 24, 2178–2191, https://doi.org/10.1175/2010JCLI3990.1, 2011.

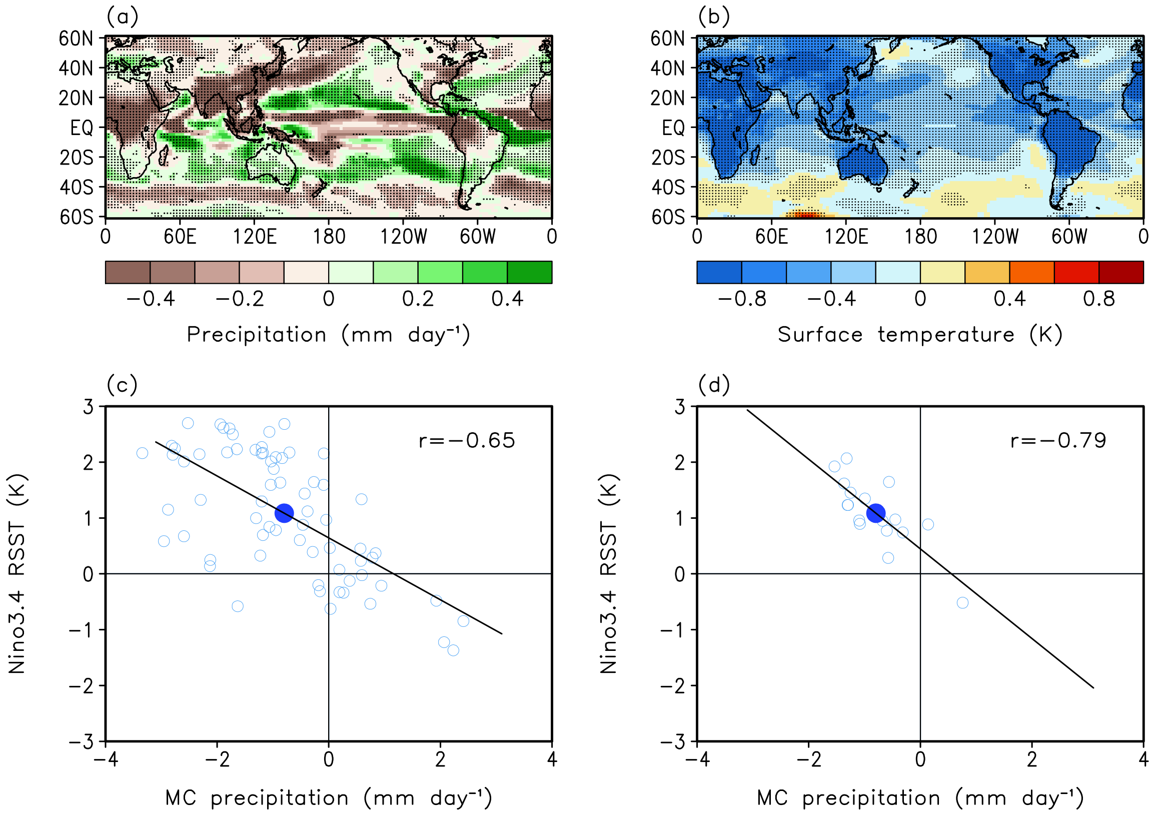

Figure S5: (a,b) Spatial pattern of (a) precipitation and (b) surface temperature anomalies during six months average following tropical eruptions. Black dots indicate the regions where the response exceeds the 95% confidence interval. (c,d) Scatter plots between post-eruption six months averaged MC precipitation and El Niño (May of YR+1 to April of YR+2) anomalies from (c) four individual tropical eruptions (n=68), (d) four tropical eruptions combined (n=17) from 17 ensemble simulations. Empty blue dots indicate each sample while filled darker blue dots indicate averages of the samples. Correlation coefficients obtained from the samples are presented together.

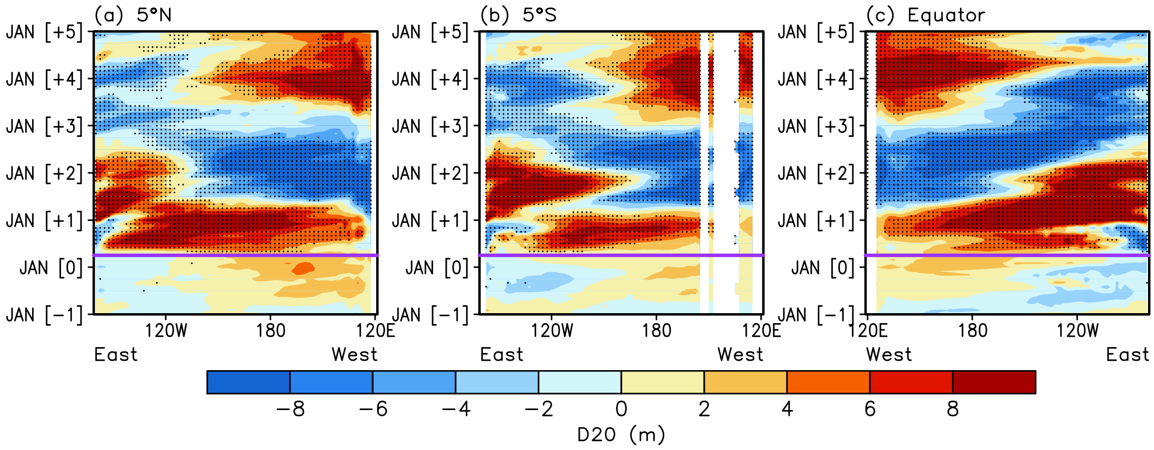

Figure S6: Same with Figs. 3c-e, but for 20°C isotherm depth anomalies.

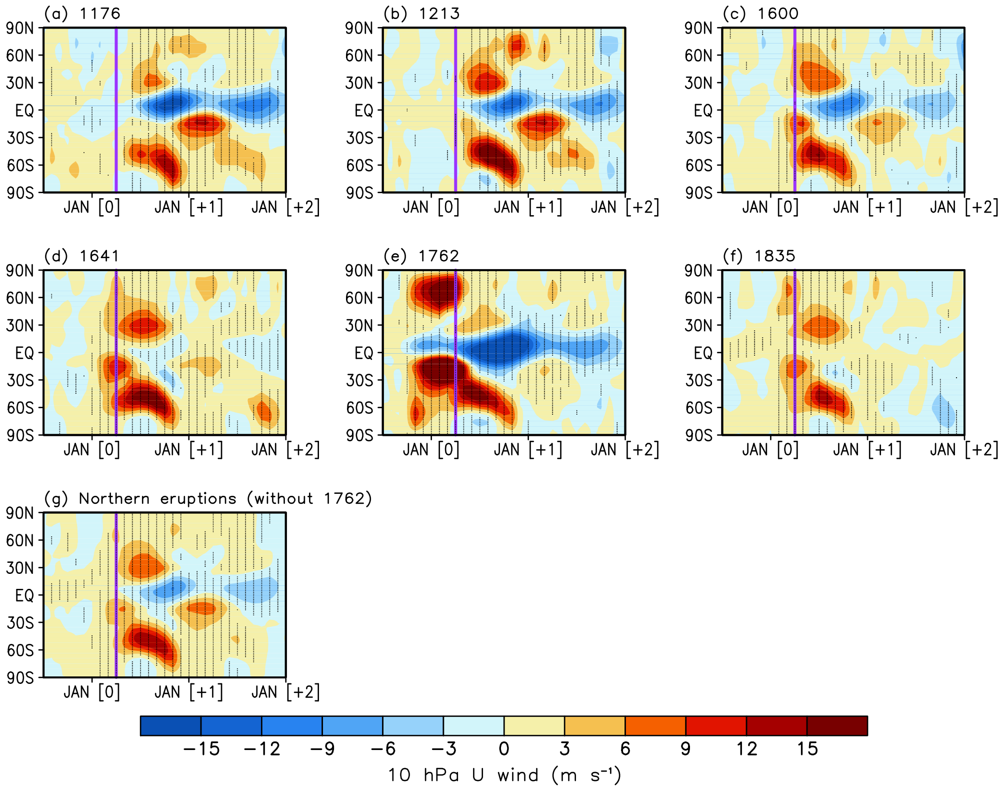

Figure S7: Same as Fig. 6d, but from (a-f) individual northern eruptions as well as (g) five northern eruptions composite without 1762 Laki eruption.

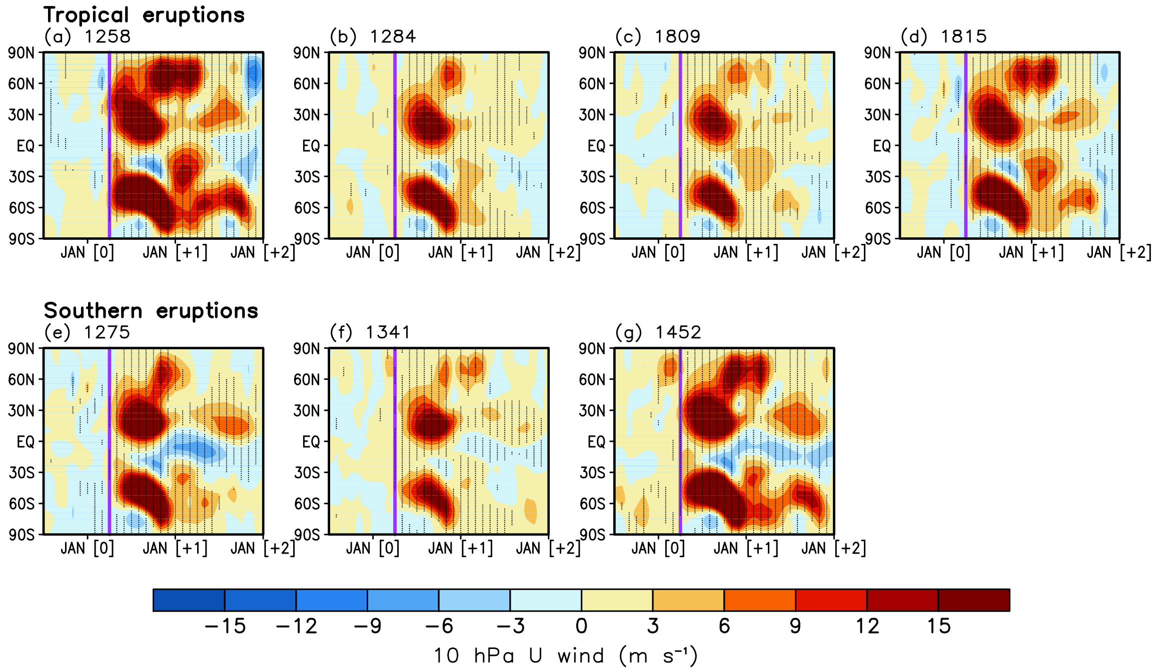

Figure S8: Same as Figs. 6b,f, but for individual (a-d) tropical, (e-g) southern eruptions.

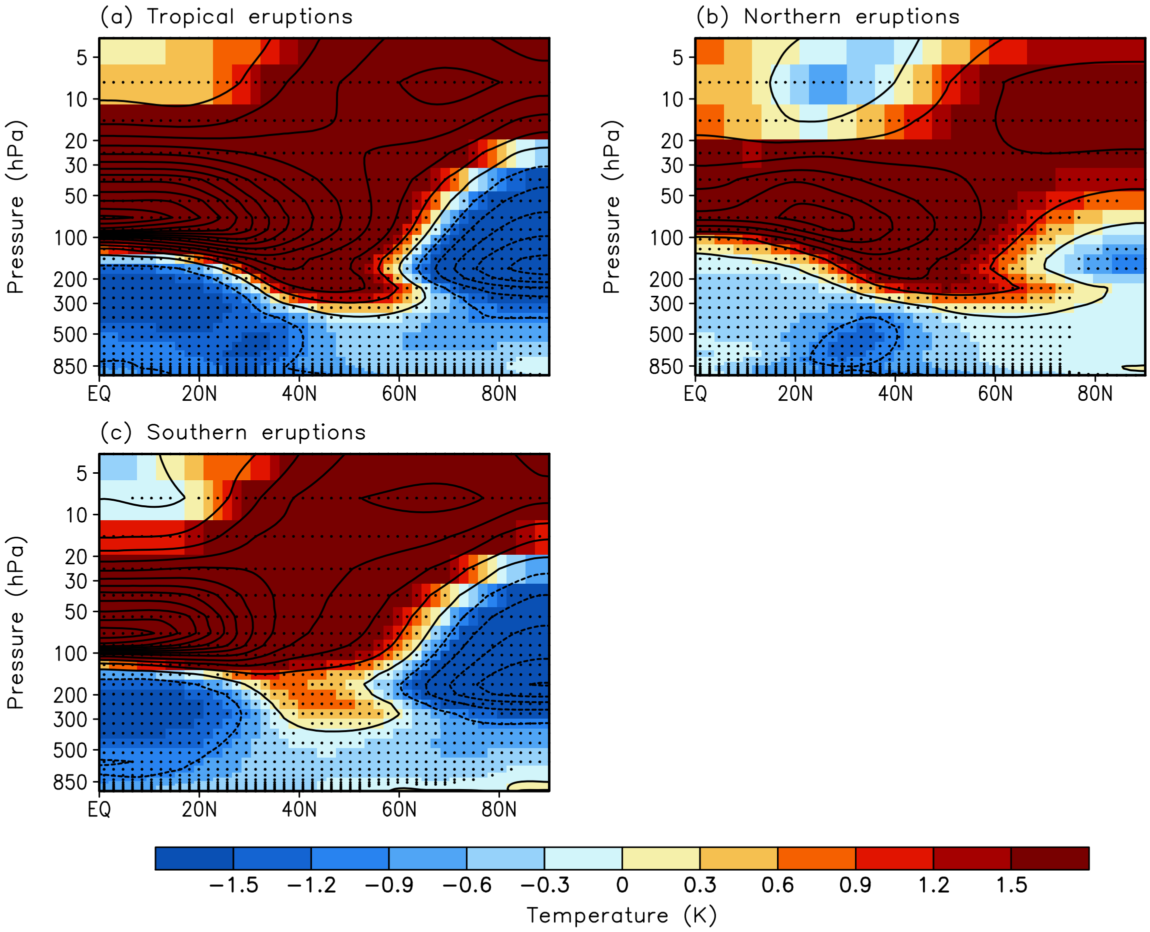

Figure S9: (a,b,c) Same as Figs. 7a,d,g respectively, but for temperature anomalies. Black contours display identical values but with 1.0 K interval.